ISSN 1063-7826, Semiconductors, 2013, Vol. 47, No. 5, pp. 686–694. © Pleiades Publishing, Ltd., 2013.
Original Russian Text © M.I. Vexler, S.E. Tyaginov, Yu.Yu. Illarionov, Yew Kwang Sing, Ang Diing Shenp, V.V. Fedorov, D. V. Isakov, 2013, published in Fizika i Tekhnika Poluprovodnikov, 2013, Vol. 47, No. 5, pp. 675–683.

PHYSICS OF SEMICONDUCTOR DEVICES

A General Simulation Procedure for the Electrical Characteristics of Metal-Insulator-Semiconductor Tunnel Structures

M. I. Vexler[a]^, S. E. Tyaginov[a,b], Yu. Yu. Illarionov[a,c], Yew Kwang Sing[d], Ang Diing Shenp[d], V. V. Fedorov[a], and D. V. Isakov[c]

[a] *Ioffe Physical–Technical Institute, Russian Academy of Sciences, St. Petersburg, 194021 Russia*
^ *e-mail: shulekin@mail.ioffe.ru*
[b] *TU Vienna, Institute for Microelectronics, Wien, 1040 Austria*
[c] *Singapore Institute of Manufacturing Technology, 638075 Singapore*
[d] *Nanyang Technological University, 639798 Singapore*

Submitted August 6, 2012; accepted for publication August 28, 2012

Abstract—The algorithm is suggested for calculating the I–V characteristics of a voltage- or current-controlled metal–tunnel-thin insulator–semiconductor system. The basic underlying physical models are discussed. Applicability of the algorithm is confirmed by a comparison of the simulation results with the measurement data obtained by the authors and borrowed from the literature, for several different structures. The presented information is supposed to suffice for calculating the electrical characteristics of the investigated structures with the various combinations of materials: metal or polysilicon gate, single-layer or stacked insulator, and semiconductor with any doping type and level.

DOI: 10.1134/S1063782613050230

1. INTRODUCTION

Metal–insulator–semiconductor (MIS) structures with a tunnel-thin insulator are important objects of investigations in semiconductor electronics. At present, such structures are considered as a one-dimensional gate cross-section of a classical field-effect transistor [1]. In addition, they have many other applications, e.g., in MOS tunnel emitter transistors [2, 3] and photodetectors [4]. The structures, in which several successive dielectric layers are used as an "insulator", are widely used in field-effect transistors (gate stacks [5]) and memory cells [6]. Among such structures are also resonant-tunnel systems based, in particular, on CaF_2/CdF_2 layers [7]. Finally, the MIS structures with thin insulator films are convenient for studying the properties of an insulating material itself. Thus, the MIS structures are extensively used.

To the best of our knowledge, there is a lack of studies that would systematize all the subproblems in simulating currents in a MIS tunnel structure. As a rule, the available are concerned with a certain important aspect with no analysis of the others. For example, the object of the recent thorough investigations has been the electron leakage current from the n-channel of a field-effect transistor into polycrystalline Si (poly-Si) [8, 9]. Meanwhile, the valence band current was even not mentioned. The most comprehensive approach to the problem was given in the studies of a MOS tunnel emitter transistor [3, 10], which, however, covered only the inversion mode of the structures.

In view of the aforesaid, it seems very important to represent algorithmically a specific calculation procedure applicable to a wide range of MIS tunnel systems. Such algorithms tested in practice would be useful when dealing with any new structure of this type, since they would make it possible to predict characteristics for the general case; the approach must be universal for any bias modes and any insulators. The aim of this study was to demonstrate such an algorithm. The physical aspects are just briefly addressed.

2. AN APPROACH TO SIMULATION OF A MIS TUNNEL STRUCTURE

In calculating the electrical characteristics of the MIS tunnel structures, the three main physical problem must always be solved.

The first problem consists in the following. Given are electric field strength F_I in the insulator and difference ΔE_{Fpn} between the quasi-Fermi levels of the silicon conduction band (E_{Fn}) and valence band (E_{Fp}). The potential distribution $q\varphi(z)$ in Si and the charge distribution are to be calculated.

The most well-known methods for calculating band diagrams are the self-consistent solution of the Schrödinger and Poisson equations [11] and the classical approach [12]. However, the first method is fairly cumbersome, while the second does not take into account the surface quantization effects. A convenient compromise seems to be the model [13, 14] that takes into account the only effective quantum level, E_0, in all

the modes, from low ($F_I < 10^6$ V/cm) to extremely high (over 10^7 V/cm) fields. Particles are often described by the wave function $\psi_0 = (b^3/2)^{1/2} z \exp[-bz/2]$ with parameter b (cm^{-1}) determined as

$$b = \left[\frac{12q^2 m_{sz}}{\varepsilon_0 \varepsilon_s \hbar^2}\left(\frac{11N_s}{32} + N_{dop} w\right)\right]^{1/3},$$

where N_s (cm^{-2}) is the concentration of induced carriers in a well, w is the band bending region width in Si, m_{sz} is the carrier effective mass, and ε_s is the permittivity of Si. Then, the level energy is

$$E_0 = \left(\frac{3}{2}\right)^{5/3}\left[\frac{q^2\hbar}{\sqrt{m_{sz}}\varepsilon_0\varepsilon_s}\right]^{2/3}\frac{N_{dop}w + (55/96)N_s}{[N_{dop}w + (11/32)N_s]^{1/3}}. \quad (1)$$

Quantities N_s and w, along with doping N_{dop}, enter the relation

$$F_I = \frac{q(N_s + N_{dop}w)}{\varepsilon_0\varepsilon_I},$$

where ε_I is the permittivity of the insulator. Such an approach is usually used for the depletion-inversion modes analyzed jointly; then, w is the depleted region width. It seems possible, however, to apply the same procedure to accumulation (although, there are more reliable methods [15]). Then, quantity N_{dop} represents the charge density on unbound states above the well; the ion charge is not taken into account due to the low ionization degree in the region of accumulation band bending. This density roughly amounts to the carrier density in the Si bulk and, consequently, to the dopant concentration. For a specified field F_I, the value of N_s is set iteratively in order to ensure the required shift ΔE_{Fpn}. The quasi-Fermi level in the bulk (E_{FB}) is determined by doping; in the well (E_{FW}), it is determined from

$$N_s = \frac{\nu_\perp m_{s\perp} k_B t}{\pi\hbar^2}\ln\left[1 + \exp\frac{E_{FW} - E_0}{k_B t}\right], \quad (2)$$

where $\nu_\perp$ is the degeneracy (the number of valleys amounts to six for electrons and three for holes) and t is the temperature. Depending on the doping type and polarity, one of the E_{FW} and E_{FB} levels is E_{Fn} and the other is E_{Fp}. The band profile is given by the formula ($z_m = \min(z, w)$)

$$q\varphi(z) = \frac{q^2 N_s}{\varepsilon_0\varepsilon_s}\left(\exp(-bz)\left[-\frac{bz^2}{2} - 2z - \frac{3}{b}\right] + \frac{3}{b}\right) + \frac{q^2 N_{dop} w}{\varepsilon_0\varepsilon_s}\left(z_m - \frac{z_m^2}{2w}\right) \quad (3)$$

and the total band bending in Si is

$$q\varphi_s = \pm q^2(\varepsilon_0\varepsilon_s)^{-1}\left(3N_s b^{-1} + N_{dop}\frac{w^2}{2}\right).$$

After N_s and E_0 are found, all the levels of light and heavy (different masses m_j) carriers can be determined, instead of one averaged level E_0. For this purpose, the quasi-classical formula

$$\int (E_{ji} - q\varphi(z))^{1/2} dz = (i - \zeta)\pi\hbar(2m_j)^{-1/2},$$

is used. The parameter ζ (equal to about 1/4) is selected such as to the sum of concentrations at the levels with the same E_{FW} would be equal to N_s. The method can be applied also to polycrystalline Si. Examples of the calculated band diagrams are given in Fig. 1.

The second problem is the following. Given are all the details of the band diagram of the MIS structure: band profiles in Si and poly-Si, voltage U on the insulator, and the quasi-Fermi level positions. Searched are the values of all the tunnel current components.

The current flowing through the insulator in the structure with a metal electrode involves the electron (metal–conduction band of the semiconductor, j_{cm}) and hole (metal–valence band, j_{vm}) components. Depending on the mode, one of these components contains only the continuous component and the other includes the additional discrete one, from the E_0 level. In the case of the polysilicon electrode, apart from currents j_{cc} and j_{vv} between the conduction and valence bands of silicon regions at high U, cross currents j_{cv} arise and the discrete component is contained simultaneously in j_{cc} and j_{vv}. Tunneling through the insulator can be combined with the transport in silicon, which broadens the range of the involved energies. At band bending in the substrate $q\varphi_s > E_g$, the band-to-band transport in Si can also take place [16]. The expression for the continuous and discrete parts of any component, whether it is $j_{cc}, j_{vv}, j_{vm}, j_{cm}$, or (for j^{cont} only) j_{cv}, is

$$j^{cont} = \frac{4\pi q\nu_\perp m_{s\perp}}{h^3}\int_{E_{min}}^{E_{max}}(f_S(E) - f_G(E))dE \times \int_0^{E_{\perp max}} T(E, E_\perp)dE_\perp, \quad (4a)$$

$$j^{disc} = \pm\frac{q\nu_\perp m_{s\perp}}{\pi\hbar^2\tau_{ar}(E_0)}\int_{E_0}^{\pm\infty}(f_S(E) - f_G(E))dE \times T(E, |E - E_0|)dE. \quad (4b)$$

Here, E is the total energy of a particle, f_S and f_G are the Fermi functions in the substrate and gate for the regions between which the transport is analyzed, $E_\perp$ is the energy in the structure plane, $m_{s\perp}$ is the particle mass where $E_\perp$ is chosen, and τ_{ar} is the time between collisions with the barrier wall (~$\hbar/E_0$). The sign in the expression for j^{disc} depends on the band ("+" for the

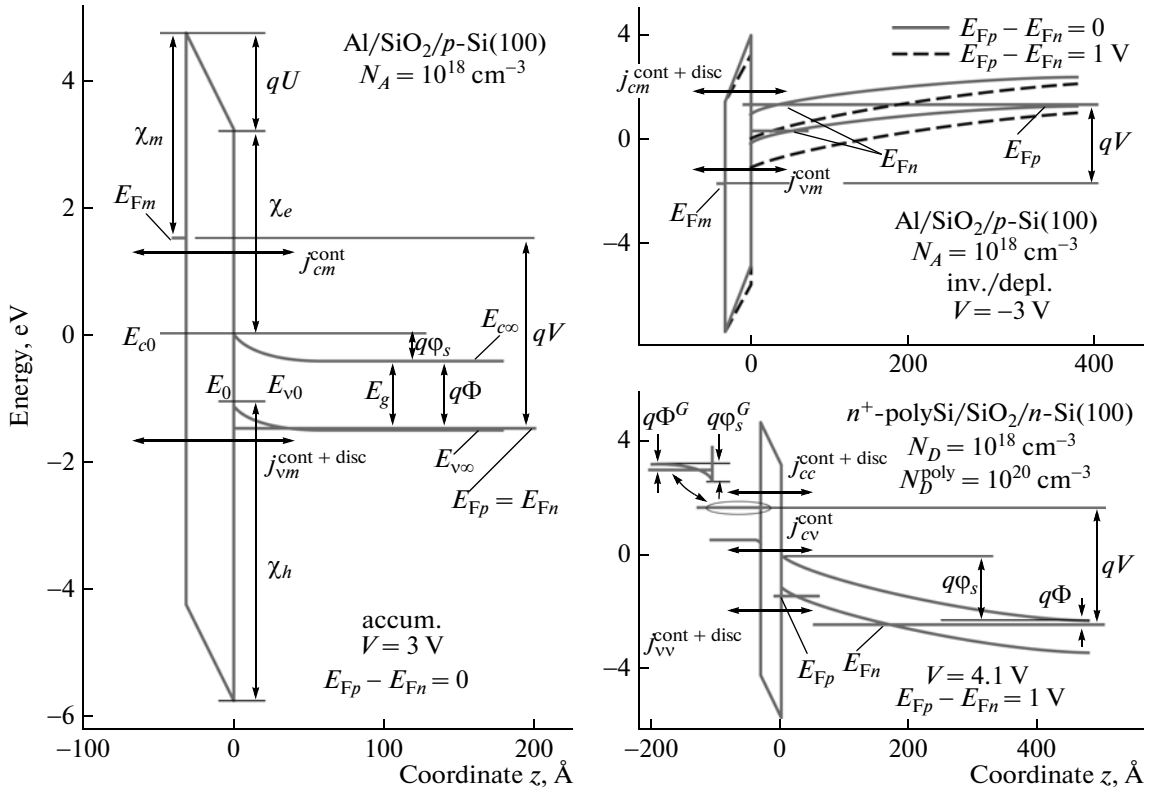

Fig. 1. Energy diagrams of the MIS structures with the quantities used in the simulation. On the left and right, the accumulation and inversion-depletion (for a metal electrode on top and for a polycrystalline one at the bottom) modes are presented.

conduction band). The limits to j^{cont} are determined by the presence of the states with the corresponding pair E and $E_\perp$ on both sides of the barrier. It is affected also by whether or not a tunneling in Si is accounted for. In particular, in Fig. 1 on the left, as applied to component j_{cm}, for j^{cont} we have $E_{\min} = E_{c0}$, $E_{\max} = +\infty$, and $E_{\perp\max} = E - E_{c0}$ for the transport via the insulator only. If we take into account also the transport in Si, then we have $E_{\min} = E_{c\infty}$ and $E_{\perp\max} = E - E_{c\infty}$. T is the tunneling probability. It is calculated by the transfer matrix method (TM) [17] or the Wentzel–Kramers–Brillouin (WKB) method [18]. The barrier region is divided into sections in which the barrier height is assumed to be constant and the integration is made by, for example, the method of rectangles. Experience shows that this is profitable even in the WKB calculations. Then,

$$T(E, E_\perp) = \exp\left[-2\Delta z \sum_i \min(k^*_{cz}(z_i), k^*_{vz}(z_i))\right], \quad (5)$$

i.e., a particle chooses the weaker barrier, top or bottom, at each point. In the case of the parabolic dispersion law in the barrier,

$$k^*_{cz} = \sqrt{2m_{cz}}\hbar^{-1}\sqrt{\max[0, (E_c - E + m_{s\perp}m_{c\perp}^{-1}E_\perp)]};$$
$$k^*_{vz} = \sqrt{2m_{vz}}\hbar^{-1}\sqrt{\max[0, (E - E_v + m_{v\perp}m_{v\perp}^{-1}E_\perp)]}, \quad (6)$$

where $m_c = m_c(z_i)$ and $m_v = m_v(z_i)$ are, generally speaking, the coordinate-dependent effective masses and $E_c = E_c(z_i)$ and $E_v = E_v(z_i)$ are the band edge energies in the corresponding element of the barrier profile fragmentation. In the case of the nonparabolic dispersion law, in particular, in the Franz model [19], k^*_{cz} and k^*_{vz} for substituting in (5) are expressed via the energies in a different way. If the barrier has the multilayer structure with intermediate wells, then the more complex TM method is required, although the formulas for the currents remain valid.

Third problem. Given are gate-substrate voltage V and (for the depletion-inversion mode in the substrate) the value of the external effect: the irradiation intensity or current j_{ext} supplied to the inversion region. Targeted are the field in the insulator and the quasi-Fermi level energy of minority carriers in the stationary situation.

Evidently, the Kirchhoff law for voltages must be satisfied,

$$\varphi_s + \varphi_s^G + U = V - V_{\text{FB}}, \quad (7)$$

where V_{FB} is the flat-band voltage. The sign of φ_s, φ_s^G, and U is positive when the field is directed toward the gate. In the case of a metal electrode, $V_{FB} = (-\chi_m + \chi_e)/q + \Phi$ (for notation, see Fig. 1); for poly-Si, we would have $V_{FB} = -\Phi^G + \Phi$. It is assumed that the quasi-Fermi levels for electrons and holes on each barrier side are independent of coordinate and always coincide in the gate and coincide in the substrate in its accumulation mode. In the case of depletion-inversion in the substrate (stationary mode), the balance is set between the lost and supplied minority carriers; the quantity ΔE_{Fpn} regulated by the MIS system itself corresponds to this balance. In the calculation, one should choose U ($|U| = F_I/d$, where d is the insulator thickness) and ΔE_{Fpn} such that they corresponded to the balance. For certainty, we consider an n-Si-based device. The minority carriers' (holes') inflow is provided by thermal generation current j_{th} proportional to depletion region width w, by photocurrent j_{ph} (often also $\sim w$), and by external current j_{ext} supplied through the source. Impact ionization is also possible: injection of each electron from the gate to the conduction band of the substrate upon flowing of current j_e (equal to j_{cm} or j_{cc}) causes the production of M-1 electron–hole pairs, which induces hole current j_e (M-1). Hole outflow from the inversion layer, except for tunnel current j_h (equal to j_{vm} or j_{vv}) is provided by diffusion–drift current j_{dd} between the interface and the bulk. We assume that the current j_{dd} is similar to the current of the p–n junction and can change its sign, becoming the hole supplier. The balance equation is written as

$$j_h + j_{dd} = j_{th} + j_{ph} + j_{ext} + j_e(M\text{-}1). \quad (8)$$

The factor from formula (8) is calculated as [20]

$$M = [1 + P(E_{inj})]\left[1 + \frac{a_0 q N_{dop} w^2}{b_0 \varepsilon_0 \varepsilon_s} \exp\left(-\frac{b_0 \varepsilon_0 \varepsilon_s}{q N_{dop} w}\right)\right], \quad (9)$$

where $a_0 = 4 \times 10^5\ \mathrm{cm}^{-1}$, $b_0 = 10^6\ \mathrm{V/cm}$, quantum yield function P is tabulated according to [21], and the injection energy is

$$E_{inj} = E_{Fm} - E_{c0} + q^2(\varepsilon_0 \varepsilon_s)^{-1}(3N_s b^{-1}).$$

Here, the last term describes the contribution of the inversion layer to the band bending. Current j_{dd} is found simply as

$$j_{dd} = A\left[\exp\frac{(E_{Fn} - E_{Fp})}{k_B t} - 1\right],$$

the preexponential factor

$$A = n_i^2 N_D^{-1}\left(\frac{(q\mu_p k_B t)}{\tau_p}\right)^{1/2}$$

contains mobility μ_p and lifetime τ_p of holes, as well as intrinsic concentration n_i. For p-Si, the approach is analogous, but we can usually assume $P = 0$.

We outlined the three basic problems arising in the simulation of the characteristics of MIS structures. In practice, they are not always solved independently, since the tunnel leakage from the inversion layer enters the balance equation.

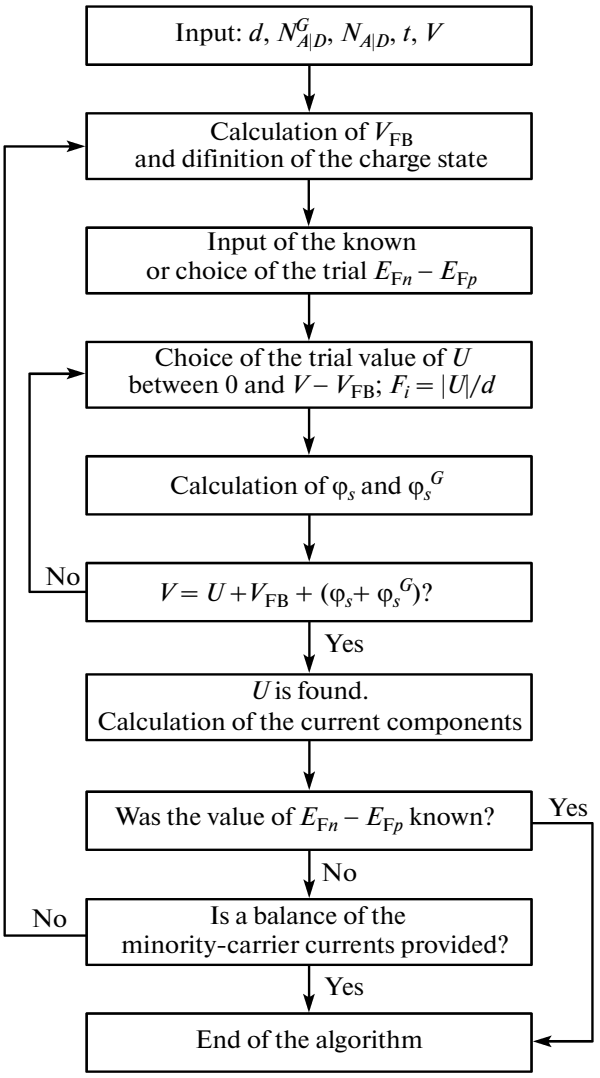

Fig. 2. Flowchart of the mathematical algorithm for calculating the I–V characteristic of the MIS structure.

3. MATHEMATICAL ALGORITHM FOR CALCULATING THE I–V CHARACTERISTIC OF THE MIS STRUCTURE

The system parameters, i.e., thicknesses of insulating layers, substrate doping level, polysilicon doping level, and orientation are assumed to be known. Dielectric constants and parameters of tunnel barriers (conduction and valence band offsets at the interface with silicon and effective masses) are also assumed to be known. In case the barrier parameters are not known with a proper accuracy the present model can be used for their determination from the measurement

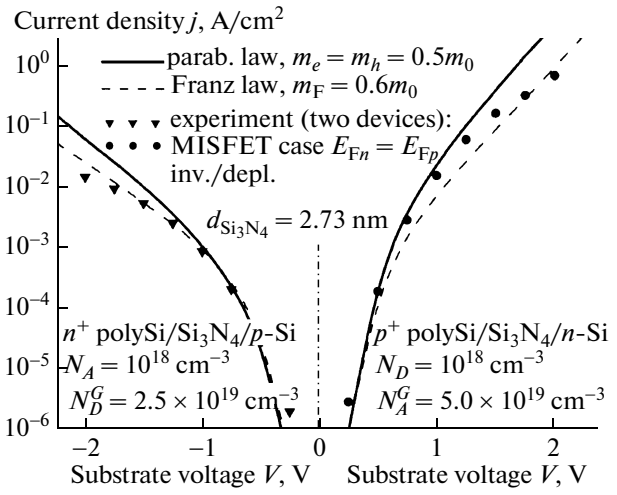

Fig. 3. I–V characteristics of the poly-Si/Si_3N_4/Si structures (depletion-inversion in the substrate). The results of the calculation with different dispersion laws are compared with the experimental data.

data like done in [10]. The effect of interface defects is not considered.

The mathematical algorithm for calculating the I–V characteristic comprises two loops. The flowchart is presented in Fig. 2. If the structure operates in the substrate accumulation mode or the difference ΔE_{Fpn} between the Fermi quasi-levels in the substrate is specified in advance, then the only one inner loop is performed. The algorithm is applicable to the simulation of devices with both metal and polycrystalline silicon gate; in the first case, the calculation is simplified, because $\varphi_s^G = 0$.

At the first step, the parameter input is made. Then, flat band voltage V_{FB} is calculated and for specified terminal voltage V, the charge states of the gate and substrate are determined. The value $E_{Fp} - E_{Fn}$ can be specified or chosen trial. Then, the trial values of voltage U on the insulator are chosen from the range between 0 and $V - V_{FB}$ and the insulator field $F_i = |U|/d$ in found. After that, band bendings $q\varphi_s$ and (for the polysilicon gate) $q\varphi_s^G$ are calculated and the equality of the sum of voltages to applied voltage V is checked over the entire structure. If the equality is valid with required accuracy, then the solution for U is considered to be obtained and the currents are calculated; if not, a new trial value of U is chosen and the loop is repeated again. If the sum of the voltage drops appears too large as compared with $|V - V_{FB}|$, then in the following iteration step $|U|$ should be reduced. As was shown in the previous section, the universal technique can be used for the accumulation and depletion-inversion modes; however, if different techniques are used, it is necessary to run individual subroutines for the loop targeting a determination of the U value.

In the variant when the value $E_{Fp} - E_{Fn}$ is specified in advance, the algorithm is accomplished when the correct value of U is found and the currents are calculated; if a trial value was chosen, then the minority-carrier current balance must be checked (see formula (8) or similar relation for p-Si). If at the found U and the calculated (with regard to j_{ph} and j_{ext}) currents, the balance condition is not met, then, it is necessary to choose another trial value of $E_{Fp} - E_{Fn}$ and repeat all the operations from the beginning.

Since in the substrate depletion-inversion mode, the same value of V can correspond to different values of $E_{Fp} - E_{Fn}$ (multistability), it is reasonable to precede the loop over $E_{Fp} - E_{Fn}$ by the calculations for the series of $E_{Fp} - E_{Fn}$ within the range from $\mp E_g$ to $q|V|$ with a small step. This will help to calculate the range(s) for the main iteration. The choice of the sign is based on the fact that the p–n junction interface–bulk should not be shifted too much in the forward direction; this imposes the limitation via E_g that excludes unrealistically large currents j_{dd}. Ignoring the multistability problem can lead to the solution loss, especially in the case of the n-substrate when the impact ionization plays an important role. Nevertheless, sometimes the scheme from Fig. 2 can be used without any additions; however, we must be confident that the ionization will not occur in a specific device (e.g. due to strong scattering on the interface) and the minority-carrier leakage will not occur in a specific device and the minority-carrier leakage current monotonically grows with $|U|$.

Extension of the calculation technique to the case of a stacked insulator (layers $d_1, d_2, \ldots, d_N$ with permittivities $\varepsilon_1, \varepsilon_2, \ldots$ and band offsets on the boundaries $\xi_{e12}, \xi_{e23}, \xi_{h12}, \xi_{h23}, \ldots, \xi_{hN-1,N}$) seems trivial. The changes will touch only the relation between voltage U on all the insulating layers and the field used in the analysis of the band bending, i.e., the solution of the first problem in the previous section. In this case, the fields of the first ($_1$) and last ($_N$) layers are used:

$$F_{1|N} = \frac{|U|}{\varepsilon_{1|N}}\left[\frac{d_1}{\varepsilon_1} + \frac{d_2}{\varepsilon_2} + \ldots + \frac{d_N}{\varepsilon_N}\right]^{-1}.$$

The presence of offsets is taken into account in the value of voltage V_{FB}.

In most cases, an iteration accuracy of 0.005 eV for qU and ΔE_{Fpn} is quite sufficient. Real barriers are almost never known with higher accuracy.

4. EXAMPLES OF THE CALCULATIONS OF THE I–V CHARACTERISTICS OF MIS TUNNEL STRUCTURES

The aim of this study was to describe and demonstrate universality of the approach for calculating the I–V characteristics of MIS structures. Therefore, for the purpose of testing, we use the data obtained

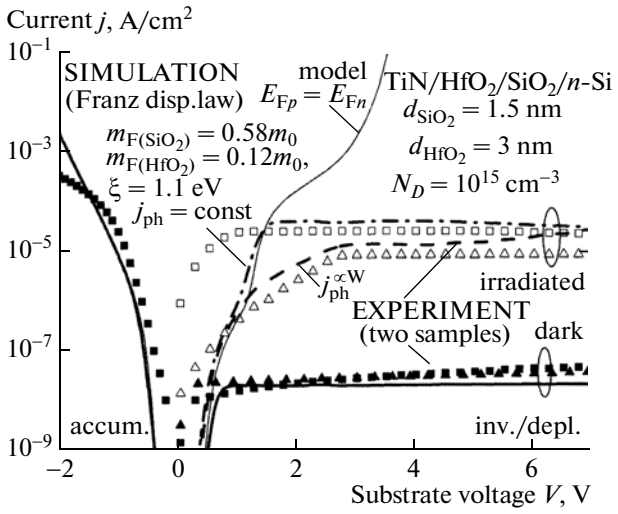

Fig. 4. I–V characteristics of the TiN/HfO$_2$/SiO$_2$/n-Si structures. For the reverse polarity, the measurement and calculation results with and without external radiation are presented.

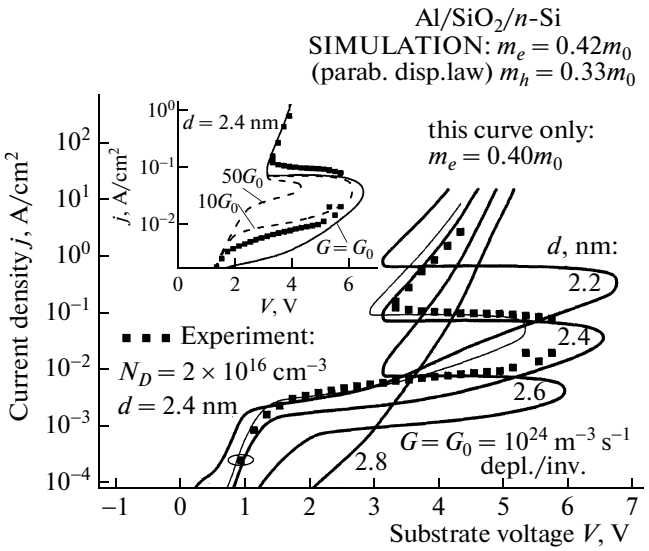

Fig. 5. Reproduction of the calculation of the S-shaped I–V characteristic of the Al/SiO$_2$/n-Si structure in the depletion-inversion mode.

for devices with three absolutely different combinations of materials: poly-Si/Si_3N_4/Si (Fig. 3), TiN/HfO$_2$/SiO$_2$/Si (Fig. 4), and Al/SiO$_2$/Si (Fig. 5). In addition, we present the results for the systems with the crystalline insulator CaF_2 (see the next section). The data for the structures with nitride were taken from the available publication [22]; the other samples were fabricated and measured by us using traditional technological and measuring techniques whose description is omitted for brevity.

Figure 3 demonstrates the I–V characteristic of the poly-Si/Si_3N_4/Si structures on n- and p-type substrates; the condition $E_{Fn} = E_{Fp}$ was intentionally kept in the field-effect transistor configuration. In this case, it is not necessary to solve minority-carrier current balance equation (8) and the situation in the presented inversion-depletion mode is close to the case of accumulation (common Fermi level), which leads to the exponential current growth with voltage. The barrier parameters are $\chi_e = 2.1$ eV [22], $\varepsilon_1 = 7.5$, and $E_{g(Si_3N_4)} = 5.1$ eV [23]. The effective masses in the insulator are given in the figure. Note that, when the Franz dispersion law is applied, the obtained theoretical I–V characteristics are more flat, which often (e.g., in Fig. 3) yields better agreement with the experiment.

The data for the TiN/HfO$_2$/SiO$_2$/Si samples are shown in Fig. 4. In the accumulation mode, the typical exponential current growth is observed. However, at the reverse polarity, in contrast to the situation in Fig. 3, the condition $E_{Fn} = E_{Fp}$ is not met. Therefore, the subproblems with finding the band diagram and tunnel currents were solved jointly. Irradiation of the structure induces generation of photocurrent j_{ph}; at strong irradiation, Eq. (8) is reduced to $j_h = j_{ph}$, i.e., the value of the tunnel leakage is determined by the photogeneration level. In this case, the tunnel current weakly depends on the voltage at the structure (Fig. 4), especially if j_{ph} is considered to be independent of the depletion region width. The constant in $j_{ph} = $ const was selected such as to obtain the best agreement. The calculation was performed for the barrier heights $\chi_e = 3.15$ eV (Si/SiO$_2$ conduction band offset), $\chi_m = 2.6$ eV (metal/HfO$_2$ barrier), $\xi = 1.1$ eV (SiO$_2$/ HfO$_2$ conduction band offset; the value is consistent with [24]), $E_{g(HfO_2)} = 6.02$ eV [25], $E_{g(SiO_2)} = 8.9$ eV and the permittivities $\varepsilon_{HfO_2} = 23$ and $\varepsilon_{SiO_2} = 3.9$. Effective mass m_F in HfO$_2$ is approximately equal to the values of m_e from [24].

In the investigated structure HfO$_2$/SiO$_2$, we practically could not enter the regimes where hot electron injection is significant. However, in the Al/SiO$_2$/n-Si system ($\chi_m = 3.17$ eV), ionization current $j_e(M\text{-}1)$ strongly affects the balance (Fig. 5). The positive feedback comes into effect: the more intense electron tunneling enhances the impact ionization, which changes the value of $E_{Fp} - E_{Fn}$, increases the minority-carrier concentration N_s, and leads to the voltage growth at the insulator, which, in its turn, enhances tunneling. As a result, the balance equation has three solutions and the I–V characteristic is S-shaped with the OFF and ON states and the negative differential resistance segment. Such a behavior was observed by us (Fig. 5) and reported in the earlier publications [3, 26]. At small thicknesses when the hole leakage is large, the S-shaped loop broadens due to a wider OFF-state branch and the inversion layer is, in fact, not formed. In contrast, at the thick insulator, component j_h is sup-

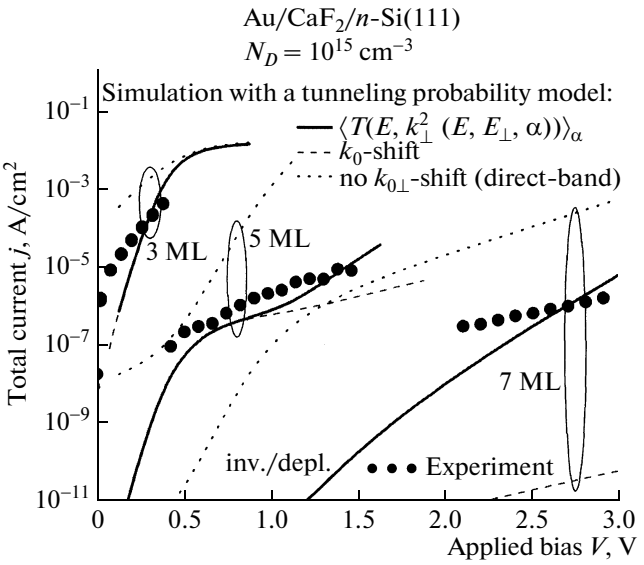

Fig. 6. *I–V* characteristic of the Au/CaF_2[3–7*ML*]/*n*-Si(111) structure in the depletion-inversion mode.

pressed; however, $j_e(M\text{-}1)$ is still significant due to asymmetry of the barrier for electrons and holes. Thus, the *I–V* characteristic is not S-shaped and the device is in the ON state. Hence, the MIS tunnel structure differs from the structures with the thick insulator not only by the presence of the current but also by the voltage distribution.

Note that the choice of the tunneling parameters is very important, since the change in the carrier effective mass even by hundredths of m_0 can noticeably change the value of the tunnel current (compare the *I–V* characteristics for $m_e = 0.40m_0$ and $0.42m_0$ in Fig. 5).

We should separately consider the issue concerning the reproduction of the dark reverse *I–V* characteristic. Most often, the lifetime in expression for j_{dd} (see after Eq. (9)) is known unreliably. In this case, it can be fitted [27] and, then, thermal generation current j_{th} may not be considered at all. Thus, for $\tau_p = 3 \times 10^{-11}$ s, the curve in Fig. 4 was reproduced. The alternative approach consists in the modeling of thermal generation current j_{th} as $qG(w - w_{V=0})$ with fitted bulk generation rate G in the substrate (Fig. 5); usually, it is $G = 10^{23}$ m^{-3} s^{-1} or sometimes higher; then the tabulated values are taken for the lifetime and j_{dd} appears very small. Parameter G, and also the lifetime, are determined by the concentration of the trap states in the band gap of the silicon substrate. The inset in Fig. 5 shows that an increase in G can noticeably narrow the bistability region.

Summarizing the results presented in Figs. 3–5, we may conclude that the technique for calculating the tunnel currents successfully works for a wide class of MIS structures. In the same manner the *I–V* characteristics of other systems, including those with stacked insulators, can be calculated.

5. ADDITIONAL PROBLEMS

Certainly, at the numerical simulation of various tunnel systems, particular problems arise. Below we touch upon two questions arising in many cases.

5.1. Crystalline Insulator: Calculation of the Transverse Wave Vector

Within the model, it was considered that transverse wave vector $k_\perp$ and energy component $E_\perp$ of a carrier in the semiconductor are related as $E_\perp = \hbar^2 k_\perp^2 / 2m_{s\perp}$. Such an approach is valid under the condition $\mathbf{k}_{0\perp} = 0$, where $\mathbf{k}_0$ is the band extremum vector, but it is applied also to the electron transport in silicon. This can be justified by the absence of pronounced differences in the currents measured in the MIS structures with oxides on Si (100) and (111), although in the first case the shift of $k_{0\perp}$ for two valleys is zero and in the second case it is fairly large ($\hbar^2 k_{0\perp}^2 / 2m_0 \approx 2.44$ eV), which should sharply reduce the tunneling probability. Possibly, at the interface between Si and the amorphous film, the wave vector with the large value relaxes [28].

Nevertheless, if the insulator is a crystal, one may expect that the tunneling process will occur with the real conservation of $k_\perp$, whatever large it is. In this case, in analyzing the transport to the conduction band of the Si (111) substrate or from it, the expression for probability T should be changed. Specifically, the expression is averaged [29] over all states α for the specified pair of E and $E_\perp$:

$$T^*(E, E_\perp) = \langle T(E, k_\perp^2(E, E_\perp, \alpha)) \rangle_\alpha \qquad (10)$$

and in formula (6), $m_{s\perp} E_\perp$ is replaced by $\hbar^2 k_\perp^2 / 2$. Near the minimum, the shift $k_\perp^2 = 2m_{s\perp}\hbar^{-2} E_\perp + k_{0\perp}^2$ [30] can be roughly introduced. For Si (100), the traditional approach $T = T(E, E_\perp)$ is used but in (4) $\nu_\perp = 2$ is put. The expressions for the current and the algorithm from Fig. 2 remain generally the same.

The example of the situation where the abovementioned tunneling features manifest themselves is the Au/CaF_2[3–7]*ML*/*n*-Si(111) structures. Figure 6 presents, along with the experimental data, the results of the calculation with regard to the real band structure of silicon with the aforementioned shift and in the direct-gap silicon approximation. Evidently, the first of the variants yields the best agreement. At low voltages, the simple shift model works not bad. The parameters used in the calculation [30] are $m_e = 1.0m_0$, $\chi_e = 2.38$ eV, $\chi_m = 2.63$ eV, $E_{g(CaF_2)} = 12.1$ eV, $G = 10^{27}$ m^{-3} s^{-1}, and $1ML = 3.15$ Å.

5.2. Inhomogeneity of the Insulator Thickness over the Area

The widely spread problem, especially in films of novel materials whose fabrication technology is not developed to the level comparable with the SiO_2 technology is related to the fluctuations of the insulator layer thickness. Due to these fluctuations, the calculated characteristics do not quantitatively correspond to the measured data, despite good qualitative agreement. In this case, in the simulation we may assume that the thickness is distributed by the Gaussian law

$$G_+(d) = (2\pi)^{-1/2}\sigma_d^{-1}\exp\left[-\frac{(d-d_n)^2}{2\sigma_d^2}\right]$$

with nominal value d_n and dispersion σ_d^2; the region $d < 0$ is ignored. The more complex Γ-type laws can also be used [31]. For deposited films (roughly, for SiO_2, too), we have $\sigma_d \approx rms$; if *rms* is measured for the layer of the same material with thickness d_{rms} different from d_n, then it should be approximately assumed that $\sigma_d = rms(d_n/d_{rms})^{1/2}$.

Usually, the conductance of the inversion or accumulated layer is rather high, so the position of the Fermi (quasi-)level of the surface quantum well can be considered equal over the entire structure area. In this case, in contrast to E_{Fp} and E_{Fn}, local voltage U on the insulator will be different for different local thicknesses d. Each component of the tunnel current is calculated as

$$j_{e|h} = \int_0^{+\infty} j_{e|h}(d, U(d))G_+(d, d_n, \sigma_n)\delta d. \qquad (11)$$

Quantities j_{th} and j_{ph} also should be weighted, since the depletion region width depends on d. In practice, if the difference ΔE_{Fpn} is given, it is convenient to calculate $j(V)$ for the thickness series in advance.

Figure 7 illustrates the comparison of the I–V characteristics of the $Au/CaF_2/p$-Si (111) structure and the results of the simulation with regard to finite standard deviation σ_d. The value of σ_d was measured using an atomic-force microscope and, in contrast to the samples presented in Fig. 6, is not negligible. The account for the inhomogeneity of the CaF_2 layer thickness significantly improves the consistence with the experiment in the depletion mode. This agreement could not be reached by fitting d = const due to the different slopes. At the same time, in the plateau segment in the depletion-inversion mode, if the current is mainly contributed to by minority carriers and therefore weakly depends on the thickness, the role of the fluctuations is less important.

It should be emphasized that any inhomogeneities are characterized by the correlation length [32], i.e., minimum distance λ between the points at which the local insulator thicknesses are independent. We considered that the relation $L \gg \lambda$ is valid, where L is the electrode size. If this condition is not met, then the spread of the I–V characteristics between the structures appear [32]. However, the average current values are independent of the ratio L/λ.

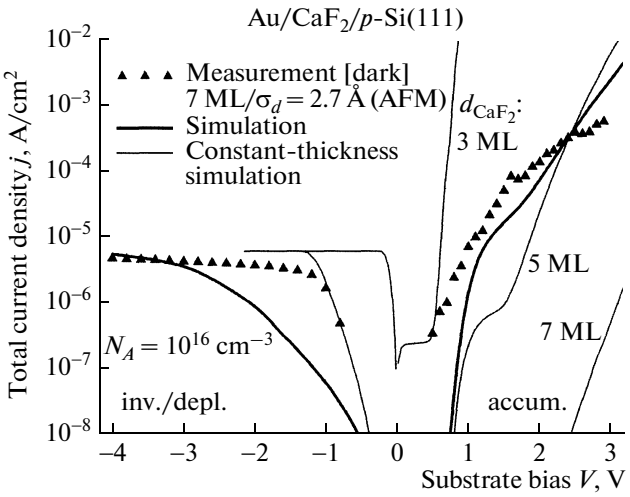

Fig. 7. I–V characteristic of the $Au/CaF_2/p$-Si(111) structure with the nonuniformly distributed thickness of the insulating layer.

4. CONCLUSIONS

The proposed general procedure of the calculation of MIS tunnel structures is applicable to the current- or voltage-controlled structures with very different materials combinations: metal or polysilicon gate, single-layer or stacked insulator, and semiconductor with any doping type and level. We described the separate subproblems and commented the basic physical models used. The important items are the universal account for the surface quantization in the accumulation and depletion-inversion modes, inclusion of the valence band current in the analysis along with the electron component, and the general record of the tunneling probability through the top and bottom barriers simultaneously. These items were partially considered in the previous studies, but the complete algorithm is presented for the first time.

We calculated the I–V characteristics of the MIS tunnel structures $Al/SiO_2/S$, $TIN/HfO_2/SiO_2/Si$, $poly\text{-}Si/Si_3N_4/Si$, and $Au/CaF_2/Si$ and reached good agreement with the experiment. The presented illustrations not only demonstrated the algorithm testing but also accented the important simulation details, such as carrier effective mass variation and the (dis)regard of the fluctuations. We believe that the information given in this work is sufficient for calculating the electrical characteristics of the structures of interest. In studying of new samples, the barrier parameters should be borrowed from the literature; the model for estimating these parameters can also be

used. Taking into account that the MIS structures are one of the most attractive objects of study in modern semiconductor physics and electronics, the general verified algorithm can be of practical importance.

ACKNOWLEDGMENTS

We are grateful to I.V. Grekhov, A.F. Shulekin, N.S. Sokolov, and S.M. Suturin (Ioffe Physical-Technical Institute) and Aye Aye and Y. Zhang (SIMTech) for help at different stages of the investigations.

Yu.Yu. I. thanks the program Erasmus Mundus for a support of the trip to Singapore.

REFERENCES

1. K. Kuhn, Ch. Kenyon, A. Kornfeld, M. Liu, A. Maheshwari, W.-k. Shih, S. Sivakumar, G. Taylor, P. VanDerVoorn, and K. Zawadzki, Intel Technol. J. **12** (12), 93 (2008).
2. E. Aderstedt, I. Medugorac, and P. Lundgren, Solid State Electron. **46**, 497 (2002).
3. E. V. Ostroumova and A. A. Rogachev, Semiconductors **28**, 793 (1994).
4. A. Ya. Vul' and A. T. Dideikin, Sensors Actuat. A **39**, 7 (1993).
5. Th. Kauerauf, B. Govoreanu, R. Degreave, G. Groeseneken, and H. Maes, Solid State Electron. **49**, 695 (2005).
6. H. Bachhofer, H. Reisinger, E. Bertagnolli, and H. von Philipsborn, J. Appl. Phys. **89**, 2791 (2001).
7. T. Kanazawa, R. Fujii, T. Wada, Y. Suzuku, M. Watanabe, and M. Asada, Appl. Phys. Lett. **90**, 092101 (2007).
8. A. Ghetti, J. Bude, P. Silverman, A. Hamad, and H. Vayda, IEICE Trans. Electron. **E83-C**, 1175 (2000).
9. N. Yang, W. K. Henson, J. R. Hauser, and J. J. Wortman, IEEE Trans. Electron. Dev. **46**, 1464 (1999).
10. I. V. Grekhov, G. G. Kareva, S. E. Tyaginov, and M. I. Vexler, Microelectron. Reliab. **47**, 669 (2007).
11. P. Palestri, N. Barin, D. Brunel, C. Busseret, A. Campera, P. A. Childs, F. Driussi, C. Fiegna, G. Fiori, R. Gusmeroli, G. Iannaccone, M. Karner, H. Kosina, A. L. Lacaita, E. Langer, B. Majkusiak, C. Monzio Compagnoni, A. Poncet, E. Sangiorgi, L. Selmi, A. S. Spinelli, and J. Walczak, IEEE Trans. Electron. Dev. **54**, 106 (2007).
12. S. Sze, *Physics of Semiconductor Devices* (Wiley, New York, 1969; Mir, Moscow, 1984), vol. 2, ch. 8.
13. T. Ando, A. Fowler, and F. Stern, *Electronic properties of two-dimensional systems* (Mir, Moscow, 1985); Rev. Mod. Phys. **54**, 437 (1982).
14. A. F. Shulekin, M. I. Vexler, and H. Zimmermann, Semicond. Sci. Technol. **14**, 470 (1999).
15. M. I. Vexler, Solid State Electron. **47**, 1283 (2003).
16. G. A. M. Hurkx, D. B. M. Klaassen, and M. P. G. Knuvers, IEEE Trans. Electron. Dev. **39**, 331 (1992).
17. B. Jonsson and S. T. Eng, IEEE J. Quantum Electron. **26**, 2025 (1990).
18. L. D. Landau and E. M. Lifshitz, *Course of Theoretical Physics*, Vol. 3: *Quantum Mechanics: Non-Relativistic Theory* (Nauka, Moscow, 1989, 4th ed.; Pergamon, New York, 1977, 3rd ed.).
19. W. Franz, in *Handbuch der Physik*, Ed. by S. Flügge (Springer, Berlin, 1956), vol. 18, p. 155.
20. S. E. Tyaginov, M. I. Vexler, A. F. Shulekin, and I. V. Grekhov, Microelectron. Eng. **83**, 376 (2006).
21. W. E. Drummond and J. L. Moll, J. Appl. Phys. **42**, 5556 (1971).
22. Y.-C. Yeo, Q. Lu, W. C. Lee, T.-J. King, C. Hu, X. Wang, X. Guo, and T. P. Ma, IEEE Electron. Dev. Lett. **21**, 540 (2000).
23. H. Yu, Y.-T. Hou, M.-F. Li, and D.-L. Kwong, IEEE Trans. Electron Dev. **49**, 1158 (2002).
24. S. Monaghan, P. K. Hurley, K. Cherkaoui, M. A. Negara, and A. Schenk, Solid State Electron. **53**, 438 (2009).
25. J. Robertson, J. Vac. Sci. Technol. B **18**, 1785 (2000).
26. S. K. Lai, P. V. Dressendorfer, T. P. Ma, and R. C. Barker, Appl. Phys. Lett. **38**, 41 (1981).
27. J. P. Shiely, PhD Thesis (Duke Univ., 1999).
28. A. Schenk, *Advanced Physical Models for Silicon Device Simulations* (Springer, Wien, New York, 1998), ch. 5.
29. Y. Y. Illarionov, M. I. Vexler, S. M. Suturin, V. V. Fedorov, N. S. Sokolov, K. Tsutsui, and K. Takahashi, Microelectron. Eng. **88**, 1291 (2011).
30. M. I. Vexler, N. S. Sokolov, S. M. Suturin, A. G. Banshchikov, S. E. Tyaginov, and T. Grasser, J. Appl. Phys. **105**, 083716 (2009).
31. W. Feller, *An Introduction to Probability Theory and its Applications* (Wiley, New York, 1967; Mir, Moscow, 1984), vol. 2.
32. S. E. Tyaginov, M. I. Vexler, A. F. Shulekin, and I. V. Grekhov, Solid State Electron. **49**, 1192 (2005).

Translated by E. Bondareva